

A multiobjective optimization approach to statistical mechanics

Luís F. Seoane^{1,2} and Ricard Solé^{1,2,3}

¹ ICREA-Complex Systems Lab, Universitat Pompeu Fabra - PRBB, Dr. Aiguader 88, 08003 Barcelona, Spain

² Institut de Biología Evolutiva, UPF-CSIC, Passg Barceloneta, 08003 Barcelona

³ Santa Fe Institute, 1399 Hyde Park Road, New Mexico 87501, USA

Optimization problems have been the subject of statistical physics approximations. A specially relevant and general scenario is provided by optimization methods considering tradeoffs between cost and efficiency, where optimal solutions involve a compromise between both. The theory of Pareto (or multi objective) optimization provides a general framework to explore these problems and find the space of possible solutions compatible with the underlying tradeoffs, known as the *Pareto front*. Conflicts between constraints can lead to complex landscapes of Pareto optimal solutions with interesting implications in economy, engineering, or evolutionary biology. Despite their disparate nature, here we show how the structure of the Pareto front uncovers profound universal features that can be understood in the context of thermodynamics. In particular, our study reveals that different fronts are connected to different classes of phase transitions, which we can define robustly, along with critical points and thermodynamic potentials. These equivalences are illustrated with classic thermodynamic examples.

PACS numbers:

I. INTRODUCTION

Most complex systems result either from evolutionary or design processes where multiple constraints must be simultaneously satisfied [1]. This includes living as well as technological and economic systems [2–13], in which very often the costs of implementing a task are confronted to its efficiency. More complicated scenarios might involve other conflicting traits as well. Optimization stands as a unifying principle that brings together questions from distant fields. The parallelisms are further highlighted by the many engineering problems that are addressed through computer-based Darwinian processes, or by the suggestion that biology *is* engineering fueled by natural selection [14].

The simultaneous optimization of several traits is usually known as *Pareto* or *Multi Objective Optimization* (MOO, [1, 15]). Given a set X composed of candidate designs or solutions $x \in X$, the challenge is to find those elements

$$x_\pi \in \Pi \subset X$$

that simultaneously optimize a series of traits

$$T_f = \{t_1, \dots, t_K\}$$

A simple example is provided by the problem of how to use a given amount of money in improving a old car. We might want to change it externally (painting and polishing the chassis) or instead invest and improve the engine. Since money places a limit to what can actually be done, the user needs to decide what type of compromise is to be achieved. In this way, the solution of an MOO ($\Pi \subset X$, the Pareto front) comprises the most optimal tradeoff between the different targets.

Previous works have been dedicated to study Pareto optimal sets [16–19] particularly in engineering and econ-

omy [15, 20, 21]. Recent work includes diverse biological systems [22–28], network models [29, 30], regulatory circuits [31–33], or control theory of complex dynamics [34, 35]. All are case-dependent, and no search for universal principles is made. However, insights into universal properties emerge as soon as we compare MOO with the physics of phase transitions. In many systems, ordered and disordered phases are separated by a transition point. Order shall result from energy minimization processes that favor neighboring particles adopting the same state. Disorder, instead, arises from noise that interfere with local ordering [36–38]. These transitions have been identified in physical, social and economic systems [39, 40]. They fall under two main classes (first or second order transitions) and display universal properties. If we can frame a MOO problem within the context of phase transitions, several powerful elements of this theory allow us to derive analytic results. In this context, statistical physics has been used in optimization problems involving a global fitness function [41–46] and their associated phase transitions [47–51]. However, little attention has been paid to the physics of Pareto optimality and in many cases multiobjective problems are reduced to a Single Objective Optimization (SOO) using global *fitness* or *energy functions* such as:

$$\Omega(t_1, \dots, t_K; \lambda_1, \dots, \lambda_K) = \sum_k \lambda_k t_k. \quad (1)$$

This approach has been used within the analysis of complex networks [6, 52–55] and models of human language [56–59]. However, different t_k might not be commensurable implying that the parameters $\{\lambda_j\}$ introduce arbitrary biases. We will avoid this linear integration initially, which is why we turn to Pareto optimality. Thanks to this we will uncover a deep connection with key thermodynamic objects [60–62]. That will reveal a series of universal features across Pareto optimal systems. These

features are tightly mapped to phase transitions (including thermodynamic ones) when the linear approach is recovered.

II. METHODS

A. Multiobjective optimization in a nutshell

This section provides a summary of key aspects of MOO that can be found in the literature [15–19]. Hereafter (and without loss of generality) we assume minimization. Consider a set X of objects upon which a minimization will be enforced (figure 1a). We refer to all objects $x \in X$ as *feasible* or *candidate solutions* or *designs*. Objects outside X are *not feasible*. Among all objects $x \in X$ we wish to find the subset $\Pi \subset X$ that minimizes a series of given, real valued mathematical features (our target functions mentioned above):

$$T_f(x) \equiv \{t_k(x); k = 1, \dots, K\}, \quad (2)$$

Our task is to find those objects that score lower in all $t_k \in T_f$ simultaneously. T_f establishes a mapping between X and \mathbb{R}^K , that we refer to as *target space* (figure 1b).

We say that a candidate solution x dominates another y (and we denote it $x \prec y$) if $t_k(x) \leq t_k(y)$ for every $k = 1, \dots, K$ and there is at least one k' such that $t_{k'}(x) < t_{k'}(y)$ (figure 1c). If a solution dominates another it is *objectively better* – i.e. *more optimal* – considering *all* targets. A solution $x \in X$ will be Pareto optimal if it does not exist any other feasible solution $y \in X$ such that $y \prec x$. The Pareto front is the set of all Pareto optimal solutions ($x_\pi \in \Pi$) of an MOO. This object is mapped into \mathbb{R}^K by T_f yielding a hypersurface $T_f(\Pi)$ of dimension $K - 1$ or lower (figure 1b). We shall refer to $T_f(\Pi)$ or Π as Pareto optimal set or Pareto front indistinctly.

In figure 1b-c we plotted a very smooth front, but more complex ones show up in real examples. Consider a Pareto optimality approach to protein structure prediction [22] (figure 1d-e). Atoms in a protein are subjected to both local forces (through their bounds with neighboring atoms) and mean-field forces such as the van der Waals potential emerging from coarse grained, distant atoms. Both contributions should be minimal at equilibrium. The Pareto efficient set of protein structures optimally trades between local and global forces and produces an effective ensemble of protein conformations. In the same vein, we could search for models of spiking neurons that simultaneously minimize their divergence with respect to different aspects of real spike trains, as in [23] (figure 1f-g). This again produces ensembles of models. In these and other cases (see [29, 30, 35]) we notice that the fronts display complex shapes, suggesting inhomogeneous accessibility to different alternative optimal solutions. As shown below, these changes in the Pareto front structure result from the presence of phase transitions.

B. Simplest SOO defined upon an MOO – MOO-SOO collapse

Given an MOO with K target functions $T_f \equiv \{t_k, k = 1, \dots, K\}$ we define the simplest SOO problem by a linear combination of the targets through a set of external parameters $\Lambda \equiv \{\lambda_k; k = 1, \dots, K\}$. This produces a global *energy function*:

$$\Omega(x, \Lambda) = \sum_k \lambda_k t_k(x). \quad (3)$$

This *energy* is an analogy, but since $\Omega(x, \Lambda)$ is minimized, global optima dwell at the minimums of a potential landscape, which results in very intuitive visualizations of our optimal systems.

The minimization of Ω for a given Λ with fixed values $\lambda_k \in \Lambda$ yields one SOO problem, thus equation 3 defines a parameterized family of SOOs. We will study i) these SOOs, ii) the constraints that the Pareto front imposes to their solutions, and iii) the relationships between different SOOs of the same family. The validity of the results holds for any positive, real set Λ but for convenience: i) We take $K = 2$, which simplifies the graphic representations and contains the most relevant situations possible. Some remarks are given about $K > 2$. ii) We require $\sum_k \lambda_k = 1$ without loss of generality. For $K = 2$ then $\lambda_1 = \lambda$, $\lambda_2 = 1 - \lambda$, and

$$\Omega = \lambda t_1 + (1 - \lambda) t_2$$

iii) We impose $\lambda_k \geq 0 \ \forall k$. The case $\lambda_k = 0$ is briefly commented.

For given λ_k , one definite SOO problem is posed. Then, equation 3 with fixed Ω defines *isoenergetic* surfaces noted $\tau_\Lambda(\Omega)$. Each $\tau_\Lambda(\Omega)$ constitutes a $K - 1$ dimensional hyperplane in the K -dimensional target space. For $K = 2$ (figure 2a) these surfaces are defined as:

$$\tau_\lambda(\Omega) \equiv \left\{ (t_1, t_2) \mid t_2 = \frac{\Omega}{1 - \lambda} - \frac{\lambda}{1 - \lambda} t_1 \right\}. \quad (4)$$

This $\tau_\lambda(\Omega)$ for $K = 2$ means that, for a fixed λ , all solutions laying on the same straight line defined by equation 4 have the same energy Ω . Solutions with lower or higher values of Ω for the same λ lay also in straight lines parallel to the original one. For general $K \geq 2$, the slope of $\tau_\Lambda(\Omega)$ along each possible direction \hat{t}_k in the target space only depends on Λ so that different $\tau_\Lambda(\Omega)$ for a given SOO problem are parallel to each other. In particular, for $K = 2$ from equation 4, we read the slope

$$\frac{dt_2}{dt_1} = -\frac{\lambda}{1 - \lambda}$$

The crossing of $\tau_\Lambda(\Omega)$ with each axis \hat{t}_k is proportional to Ω . (figure 2a) With λ_k given and constant, minimizing Ω means finding $\tau_\Lambda(\tilde{\Omega})$ with $\tilde{\Omega}$ the lowest value possible such that $\tau_\Lambda(\tilde{\Omega})$ still intersects the Pareto front.

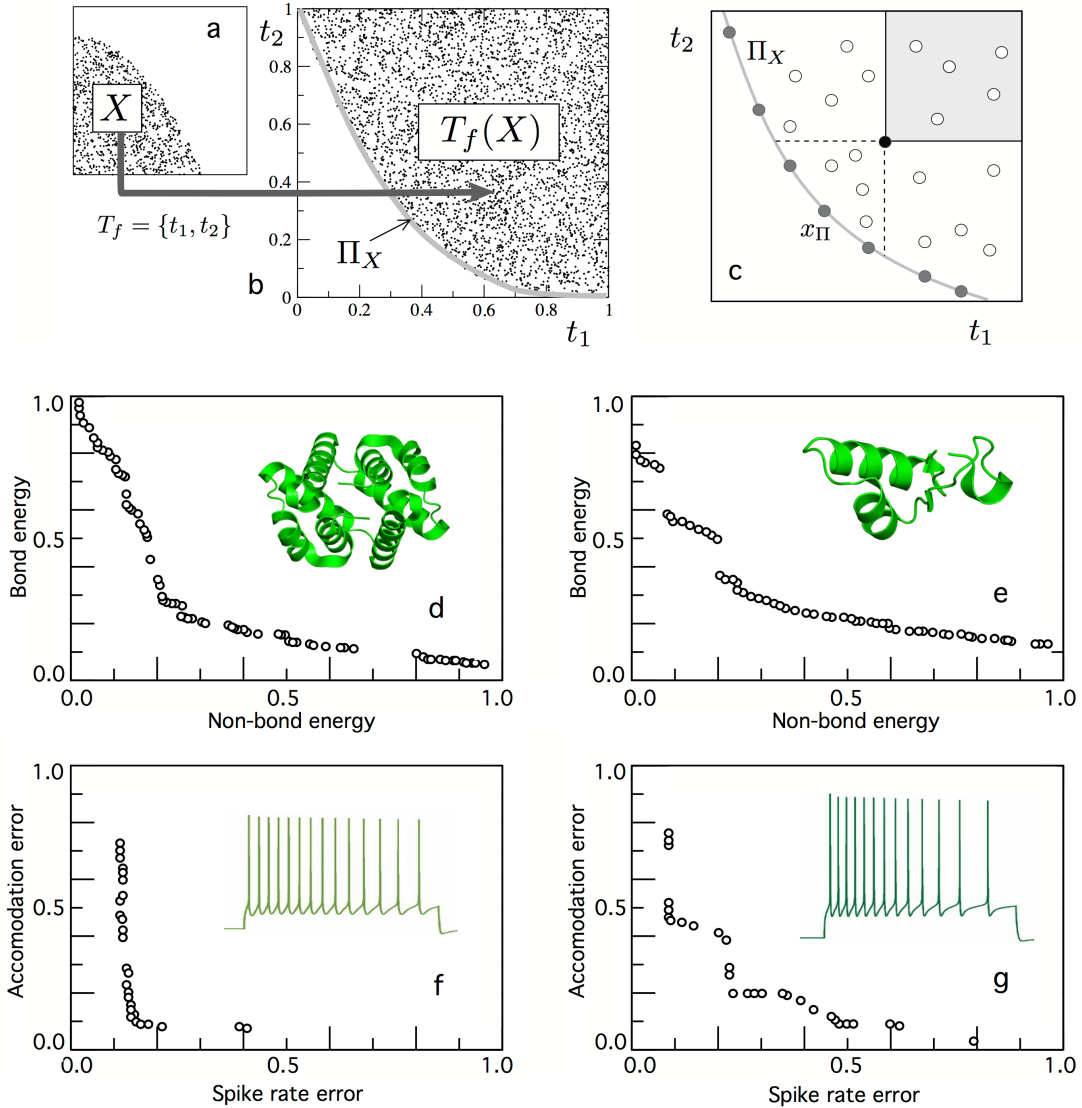


FIG. 1: **Pareto optimality and Pareto front diversity** (a) A general picture of the way the Pareto front Π_X is constructed by mapping from the space X to the target space (b) where a new cloud of points $T_f(X)$. The boundary of this cloud defines Π_X (gray line). Within the previous cloud, different types of solutions can be identified. In (c) we indicate with an arbitrary filled circle a non-optimal solution that dominates some others (within the gray square) and is dominated by others, delimited between the two dashed lines. All open circles involve non-Pareto optimal solutions. The Pareto front defines the limits of what is feasible. In (d-e) we show two examples of Pareto fronts obtained from evolved protein structures (adapted from [22]) and in (f-g) two additional examples of evolved firing neuronal patterns to fit experimental data (adapted from [23]). For convenience, we have normalized all axes. Notice the diverse structure of the fronts and the presence of changing curvatures, gaps and kinks.

Graphically, this is equivalent to *pushing* the isoenergetic surfaces against the Pareto front as much as possible (figure 2a). Hyperplanes with lower Ω exist, but the Pareto front sets the limit of feasibility: any solution with $\Omega < \tilde{\Omega}$ cannot be physically realized. The SOO optimum always lays on the Pareto front. (Take $z \notin \Pi$, then $\exists x \in \Pi$, $x \prec z$; thus at least for one $k' \in \{1, \dots, K\}$ we have $t_{k'}(x) < t_{k'}(z)$, implying $\Omega(x, \Lambda) < \Omega(z, \Lambda)$ and

z cannot be SOO optimal.)

The SOO optimum usually lays at the point $x_{\Lambda} \in \Pi$ where $\tau_{\Lambda}(\tilde{\Omega})$ is tangent to the Pareto front (figure 2a). Exceptions to this constitute the most interesting cases. The solution to different SOOs (defined by different values of λ) are found in different points along the front (figure 2b). The relationships within a family of SOO problems is thus partly encoded in the surface geometry.

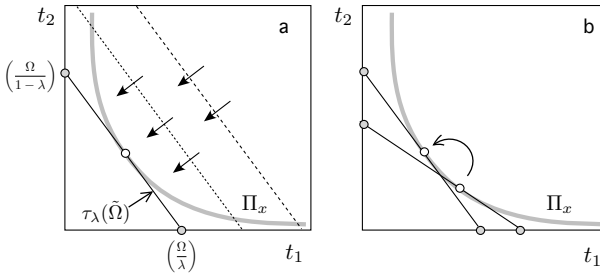


FIG. 2: **From single to multi-objective optimization.** (a) When a single-objective optimization assumption is made, a linear relation is defined between the target functions through an energy function $\Omega(\lambda) = \lambda t_1 + (1 - \lambda)t_2$ (see text). For a fixed λ one sole SOO is posed whose solution lies where $\tau_\lambda(\Omega)$ (straight lines with slope $d = -\lambda/(1 - \lambda)$) matches the tangent of the front. (b) By changing λ , we visit other solutions of the same SOO family.

C. Concavity/convexity and order parameters

The results that follow rely on a notion of concavity and convexity. The target surfaces $\tau_\lambda(\Omega)$ introduce a preferred direction along which minimization proceeds. This provides a notion of *more* and *less* optimal (*lower* and *higher* energy) so that concavities and convexities are consistently defined.

Besides, the following results deal with phase transitions that are reflected in *order parameters*. These represent some quality of our optimal designs that varies as a response to *control parameters* – these will be the biases $\{\lambda_j\}$. When phase transitions are present, these responses happen in very characteristic ways.

As for order parameters, we admit any physical, geometrical, topological, or any other features that we can measure on the elements of X . We just require i) that they make different phases distinguishable (they would be poor order parameters otherwise) and ii) that non-trivial behaviors arise out of the optimization dynamics exclusively – if not, we might encounter order parameters that become singular for some mathematical reason not relevant to our study. If the chosen indicators obey these conditions, then the singularities that we call phase transitions arise *for all* order parameters simultaneously.

For an arbitrary order parameter θ the first condition implies that if $x, y \in X$ are mapped into the same point ($T_f(x) = T_f(y)$), then $\theta(x) = \theta(y)$. The opposite ($\theta(x) \simeq \theta(y) \Rightarrow T_f(x) \simeq T_f(y)$) is only required whenever $x \not\sim y$ and $y \not\sim x$. This last condition guarantees that two points with different values of the order parameter are never mapped into the same point of the Pareto front in \mathbb{R}^K . The second condition is satisfied for θ such that $x, y \in X$ with $T_f(x) = T_f(y) + D\mathbb{R}^K$ implies $\theta(x) = \theta(y) + D\theta$, $D\mathbb{R}^K$ and $D\theta$ standing for arbitrary differential modifications. Then θ will not present

non-analyticities other than those revealed by the theory above. Following these conditions, the $t_k(x)$ themselves are valid order parameters.

III. RESULTS

A. Importance of the shape of the Pareto front

The most simple interplay between our MOO and the corresponding family of SOOs happens when the Pareto front is convex and its tangent in the $\hat{t}_1 - \hat{t}_2$ plane is well defined in its interior and its slope spans the interval $(-\infty, 0)$ (figure 2a). Then, the solution to the SOO posed by a given λ is always found where the Pareto front has slope $d = -\lambda/(1 - \lambda)$ and $\tau_\lambda(\tilde{\Omega})$ matches the tangent of the front. A differential increase $\lambda \rightarrow \lambda + D\lambda$ modifies the slope:

$$d \rightarrow d + \frac{2\lambda - 1}{(1 - \lambda)^2} D\lambda$$

of the $\tau_\lambda(\tilde{\Omega})$. For $\lambda \in (0, 1)$, $d \in (0, -\infty)$. Each λ poses an SOO with a different solution. Varying λ , successive SOO solutions *roll smoothly* over the front (figure 2b). This is similar to laying a rigid straight line ($\tau_\lambda(\tilde{\Omega})$), indeed) against the front and reading the solution for different inclinations of the $\tau_\lambda(\tilde{\Omega})$ at the contact point between that rigid line and the front. Any order parameter θ renders a continuous, differentiable function of λ .

a. Second order phase transitions In figure 3a, b, and c we represent convex Pareto fronts whose slopes span $d \in (-\infty, d^*)$, $d \in (d^*, 0)$, and $d \in (-\infty, d^-) \cup (d^+, 0)$ respectively (with $-\infty < d^*, d^-, d^+ < 0$). In all cases we find convex stretches of the front with well defined tangents limited by points with sharp edges. Using $\lambda = -d/(1 - d)$ we reveal the intervals $\lambda \in (\lambda^*, 1)$, $\lambda \in (0, \lambda^*)$, and $\lambda \in (0, \lambda^+) \cup (\lambda^-, 1)$ respectively. For these intervals a series of SOO problems exist whose solutions are always found where the $\tau_\lambda(\tilde{\Omega})$ match the tangent of the front. These can be smoothly visited as λ changes infinitesimally slow, just as before.

Consider now figure 3a for $\lambda \in (0, \lambda^*]$. We can define SOO problems in this range, but an abrupt ending of the front (nowhere does its slope match $d = -\lambda/(1 - \lambda)$ for $\lambda \in (0, \lambda^*]$) implies that the solution to all these SOOs is the same. This is indicated by the gray fan in figure 3a: a collection of isoenergetic surfaces ($\tau_\lambda(\Omega)$) with different inclinations has been pushed all the way against the front arriving to one same solution. This happens also in figures 3b-c: several isoenergetic surfaces (those with $\lambda \in [\lambda^*, 1]$ and $\lambda \in [\lambda^+, \lambda^-]$ respectively) reach the same solution when pushed against the front. As we vary λ within these relevant intervals any order parameter remains unchanged ($\frac{d\theta}{d\lambda} = 0$) because we report persistently the same solution. But these same order parameters change at non-zero rates as we approach $\lambda^{*,\pm}$ from the outside. Because every point of the front can be

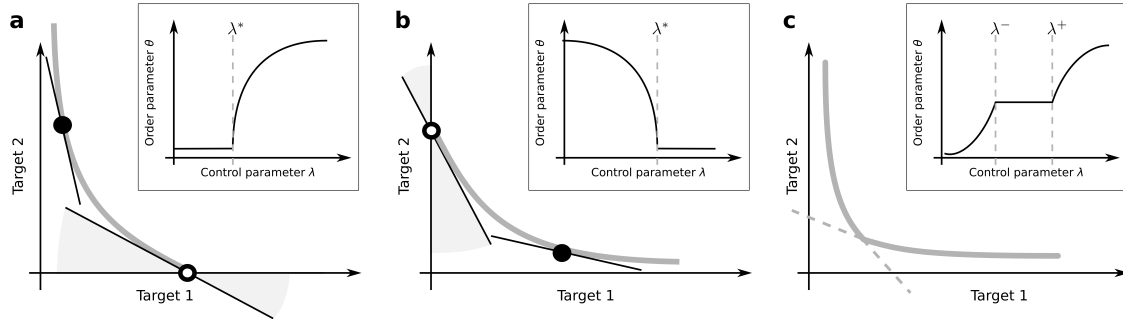


FIG. 3: **Convex Pareto front with a tangent whose slope does not span the whole range $(-\infty, 0)$.** **a** The slope of the Pareto front spans $d \in (-\infty, d^*)$. The front *ends abruptly* at its bottom-right. There is a range ($\lambda < \lambda^*$, with $\lambda^* = -d^*/(1-d^*)$) indicated by the gray fan) for which well defined SOO problems exist, whose solution is persistently the same (open circle). For $\lambda > \lambda^*$ (filled circle) the front is sampled gently as before. Any order parameter θ (inset) does not change if $\lambda < \lambda^*$ because the SOO optimum remains unchanged. Its derivative is not zero for $\lambda > \lambda^*$. This causes an abrupt shift in $\frac{d\theta}{d\lambda}$ at λ^* while $\theta(\lambda)$ remains continuous. **b** The exact same situation happens if the pathology is found at the top-left of the front. **c** A sharp edge is associated with two discontinuities in the derivative of any order parameter.

reached for some λ , plotting θ (figure 3, insets) produces a continuous curve while there must be a discontinuity in the derivatives. This is the fingerprint of **second order phase transitions** and is coherent with an interpretation based on the thermodynamic Gibbs surface [61, 62].

b. First order phase transition In thermodynamics, discontinuous transitions and metastability are associated to concavities in the Gibbs surface [61, 62]. The same is true about Pareto optimal designs, for which the Pareto front is equivalent to the Gibbs surface.

In a fully concave front (figure 4a), the straight line that joins both ends of the front has slope d^* and defines a critical value $\lambda^* \equiv \frac{-d^*}{1-d^*}$. The solution to any SOO with $\lambda < \lambda^*$ sits at the bottom-right end of the front. For $\lambda > \lambda^*$ the solution lays at the top-left end. Both extremes coexist for $\lambda = \lambda^*$. We cannot roll smoothly over such front by varying λ . A sudden shift between radically different optima happens at λ^* . Any order parameter remains constant below and above λ^* but a gap exists between both constant values (figure 4a, inset), as in first order phase transitions. Similar gaps are revealed when concavities are embedded within convex stretches of the front (figure 4b-c). Global optima always lay on the convex hull of the Pareto front. Pareto optimal designs inside the cavity might be metastable – i.e. local optima – but are never global SOO optima. Metastability leads to the existence of hysteresis loops.

A final illustration of first order phase transitions comes through the energetic landscape enforced by $\Omega(x, \lambda)$ (figure 4d). For different values of λ we computed $\Omega(x, \lambda)$ for every Pareto optimal solution of the front in figure 4c. This renders an energetic boundary (thick black curves) below which feasible solutions do not exist (gray areas cannot be accessed). Heavy marbles rolling down the potential wells minimize their energy. Metastability and hysteresis dynamics are due to changes in the potential landscape (i.e. in the underly-

ing SOO problem): As λ varies a new pocket becomes locally stable (figure 4d, $\lambda = 0.3$) and grows until it becomes the global minimum ($\lambda = 0.43$ through $\lambda = 0.5$). We might get stuck in the new local minimum until it is destabilized ($\lambda = 0.8$).

c. Other situations Phase transitions are among the most interesting phenomena accounted for by the Pareto front, which generalizes the Gibbs surface for the studied MOO-SOO systems. Because of the equivalence between both objects, we remit the reader to more specialized literature to discuss the more technical details [65–67].

If the front contains a straight segment in the feature plane we define a critical value $\lambda^c \equiv \frac{-d^c}{1-d^c}$ with d^c the slope of the segment. In figure 5a a situation similar to the first order phase transitions from figure 4a is found with either extreme of the front solving the SOOs defined by $\lambda \gtrless \lambda^c$ respectively. Besides, any Pareto optimal design is SOO optimal at this critical value. Hence, at $\lambda = \lambda^c$ a plethora of very heterogeneous solutions not visited under any other circumstance becomes available. Straight stretches of the front might also happen along second order phase transitions (figure 5b). In all these cases the derivative of order parameters with respect to λ diverges for $\lambda \rightarrow \lambda^c$, as in critical points.

$\lambda = 0$ is the only situation in which solutions not in the Pareto front solve an SOO (figure 5c). At least one of these solutions must be Pareto optimal. This case is straightforwardly incorporated in the general framework, so allowing $\lambda_k = 0$ does not alter our theory.

We assumed that the λ_k are the only relevant control parameters, but other external variables may modify the shape of the front or its elements. This could prompt phase transitions into existence or erase them. (This can also be due to the varying of some λ_k if $K > 2$, as noted for the Gibbs surface [67].) Parameters changing the constituents of the front could trigger drastic changes not studied here.

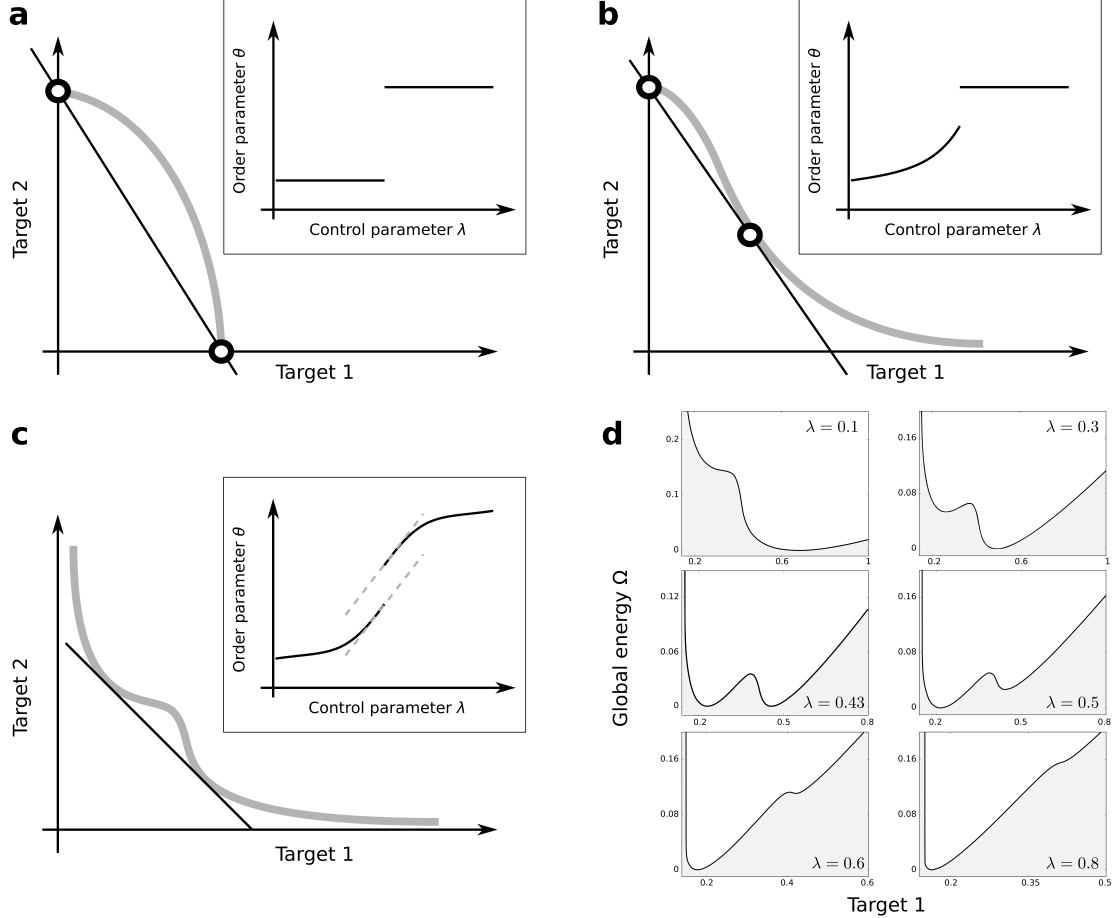


FIG. 4: **Concave Pareto front, or fronts with concavities.** **a** Only two solutions are ever SOO global optima in a concave front: one if $\lambda > \lambda^*$ and another if $\lambda < \lambda^*$. For $\lambda = \lambda^*$ both solutions coexist. Any order parameter presents a sharp discontinuity at $\lambda = \lambda^*$. A similar situation happens in **b** and **c**. In the later case, while $\theta(\lambda)$ is not continuous, its derivative is. **d** An *energetic landscape potential* is built through equation 3. Plotting this function for all the points of the front in **c** reveals an energetic boundary below which no solutions exist. Pareto suboptimal solutions lay above the boundary and SOO optima at fixed λ sit at the bottom of energy wells. Metastable solutions are associated to local minima and lead to hysteresis if we change λ back and forth.

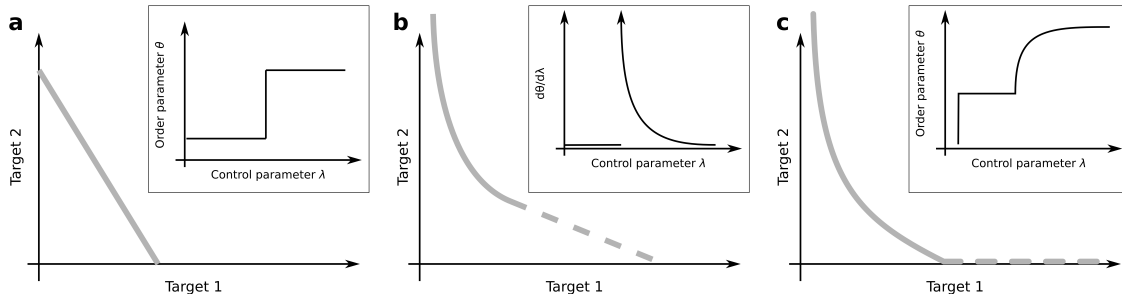


FIG. 5: **A straight segment in the front resembles criticality.** **a** A situation similar to first order transitions for $\lambda \leq \lambda^c$. At λ^c the whole front is SOO optimal. **b** Degenerated SOO solutions can also happen at second order phase transitions implying a diverging derivative in any order parameter. **c** The dashed segment is not Pareto optimal but it becomes SOO optimal if $\lambda = 0$ is allowed.

B. Thermodynamics as a multiobjective optimization problem

We intend that phase transitions for MOO-SOO problems are as firmly grounded as those in statistical mechanics, so we proceed now to show how thermodynamics is included in our theoretical framework. Take an arbitrary physical system that can occupy any state σ_j of an arbitrary, abstract space $\sigma_j \in \Sigma$. Each σ_j is a physical configuration with energy E_j . Consider an arbitrary ensemble for this system P_i , in which σ_j shows up with probability $P_i(\sigma_j)$. Consider, indeed, all possible ensembles P ($P_i \in P$), each of them an arbitrary, mathematically consistent probability distribution, i.e.

$$\sum_j P_i(\sigma_j) = 1,$$

over the space Σ . We define the functions:

$$\begin{aligned} U(P_i, \Sigma) &= \sum_j P_i(\sigma_j) E_j, \\ S(P_i, \Sigma) &= - \sum_j P_i(\sigma_j) \log(P_i(\sigma_j)); \end{aligned} \quad (5)$$

i.e. the internal energy and entropy of each ensemble P_i . These functions are rigorously defined irrespective of whether they bear any physical meaning. Since the P_i are arbitrary probability distributions there is not any guarantee (neither necessity, so far) that $U(P_i, \Sigma)$ or $S(P_i, \Sigma)$ obey any relevant relationship.

These functions map $P_i \in P$ into the $U - S$ plane (\mathbb{R}^2), where dominance and Pareto optimality are well defined. We can find the subset $\Pi \subset P$ of probability distributions $P_\pi \in \Pi$ that minimize $U(P_i, \Sigma)$ and maximize $S(P_i, \Sigma)$ simultaneously. This is a legitimate MOO problem, again irrespective of whether it has got any physical relevance. The only difference with earlier MOOs is that one of the targets is maximized, which does not alter any of our conclusions. The solution to this problem ($P_\pi \in \Pi$) constitutes the optimal tradeoff between the targets in equation 5. This reduces the number of relevant ensembles for us, but still there is no guarantee nor any need that these $P_\pi \in \Pi$ present notable physical properties. They are just probability distributions solving an ad-hoc MOO.

Consider now the family of SOOs defined by:

$$\begin{aligned} \min \left\{ \Omega(U, S; \lambda_U, \lambda_S) \equiv \lambda_U U + \lambda_S S \right\} &\Rightarrow \\ \Rightarrow \min \left\{ \hat{\Omega} \equiv \frac{\Omega}{\lambda_U} = U + \frac{\lambda_S}{\lambda_U} S \right\}. \end{aligned} \quad (6)$$

This collapses the original MOO into a series of SOOs whose solutions lay upon the convex hull of Π in the $U - S$ plane, as shown above, so that phase transitions arise for singular values $(\lambda_U/\lambda_S)^{*,\pm}$ due to concavities and sharp edges of the corresponding front. These are still phase transitions of a fabricated problem.

We leave this artificial MOO aside for a while. We can find the ensembles that maximize S for fixed values of

U , as dictated by the second law for equilibrium thermodynamics. These distributions correspond to the microcanonical ensembles that can be mapped into the $U - S$ plane through equation 5 describing a curve. For each fixed U we attain the maximum possible S , thus reconstructing the Pareto front of the MOO above (see SM). Irrespective of whether thermodynamics consists in an MOO, microcanonical ensembles are linked to the Pareto front of a legitimate MOO.

The laws of thermodynamics also imply that

$$F = U - TS = U - S/\beta \quad (7)$$

is minimized in equilibrium at fixed temperature [62]. Thermodynamic canonical ensembles embody this minimization. Identifying $\hat{\Omega} \equiv F$ and $\lambda_S/\lambda_U \equiv -T = -1/\beta$ from equations 6 and 7, the relevant $(\lambda_U/\lambda_S)^{*,\pm}$ correspond to those temperature values at which phase transitions occur. Irrespective of whether thermodynamics consists of an MOO-SOO collapse, canonical ensembles are constrained by the rules that reveal phase transitions in one such system. First order phase transitions are associated to cavities at which the Pareto front and its convex hull (i.e. microcanonical and canonical ensembles) must differ. This is in agreement with recent literature in *ensemble inequivalence* [68] some of whose results can be intuitively derived in our framework.

As a final remark, thermodynamic systems described by internal energy, entropy, and volume find their microcanonical ensembles laying at the more general surface defined by the Gibbs potential $G = U - TS - pV$ [61, 62]. This also corresponds to the Pareto front of an MOO problem. Phase transitions are then identified for singular values of temperature and pressure (see SM).

The Ising and Potts models illustrate second and first order transitions respectively. General versions of these models have been solved using ensemble inequivalence [69, 70]. They are discussed here because they allow an almost complete analytic resolution using the methodology and vocabulary of MOO (see SM for details). The Ising model presents a convex Pareto front (figure 6a). This front results in a function $S = \bar{S}(U)$ well defined for $U \in [-Jz/2, 0]$, J being the coupling constant of the model and z the number of nearest-neighboring spins. Because entropy is maximized (as opposed to the minimizations in previous sections) the Pareto front has positive slope. Apart from this, exactly as solutions for SOOs with fixed λ were found where the slope d of the front matched $d \equiv -\lambda/(1 - \lambda)$, now solutions for fixed β are associated to some slope $d(\beta)$. We get curves of constant free energy $\tau_\beta(F)$ just as we got isoenergetic surfaces $\tau_\lambda(\Omega)$ before:

$$\tau_\beta(F) = \left\{ (U, S) \mid S = \beta U - \beta F \right\}. \quad (8)$$

The free energy minimization is equivalent to pushing these $\tau_\beta(F)$ as much as possible against the front without changing its slope (i.e. without changing β , thus at constant temperature). This reveals how SOO solutions are

found now precisely where $\partial S/\partial U = d = \beta$. The derivative $\partial \bar{S}/\partial U$ tends to $+\infty$ for $U \rightarrow (-Jz/2)^+$, meaning that this end of the front is only reached for $\beta \rightarrow +\infty$ (i.e. $T \rightarrow 0$). Nothing remarkable happens there. At the other end of the front $\partial \bar{S}/\partial U$ tends to $1/Jz$ for $U \rightarrow 0^-$. Thus, the range $\beta \in (1/Jz, 0]$ (gray fan in figure 6a) defines SOOs whose solutions are always the most entropic configuration of the Ising model. At $\beta \geq 1/Jz$ the SOO solution leaves the disordered phase towards the ordered, magnetic one.

The Potts model (its front and a sample of not Pareto-optimal solutions is shown in figure 6b) presents a concavity in the top-right end of its Pareto front as revealed by the derivative dS/dU , which is not monotonously decreasing (figure 6c). This implies a first order phase transition from the most entropic configuration to the ordered state, as it is known [71]. Calculations based on the convex hull of this front match those obtained elsewhere [72] (see SM). Again, nothing remarkable happens at the lower left end of the front, which is reached for $\beta \rightarrow +\infty$ ($T \rightarrow 0$).

IV. DISCUSSION

In this paper we presented a theoretical framework to discuss Pareto optimal systems that collapse into families of SOOs. We have uncovered deep equivalences of key objects in MOO (the Pareto front) and fundamental concepts of thermodynamics (the Gibbs surface) [60–62]. Consequently, a firm basis exists to extend this physical theory to a wider collection of MOO-SOO systems.

An important motivation of our paper was to find broad regularities based on the general structure of the optimization problems, without regard of what is being optimized in each particular case. Given two different problems that happen to have the same Pareto front, we automatically know that both systems undergo the same phase transitions: in both systems they will have the same order (first or second) and location in control parameter space. Only their physical or geometrical interpretations will differ. The most important contribution of this paper is from thermodynamics towards the investigation of Pareto optimal systems. The possibility of defining effective potentials associated to the Pareto front go hand in hand with the first and second order transitions revealed.

By considering the theoretical framework developed in this paper, these kind of analyses are easily available (and absent, to the best of our knowledge) for other Pareto optimality research. This, we believe, enriches the interpretation of Pareto efficient systems. Take the example mentioned above involving the minimization of short- vs. long-range forces in protein structure [22]. The fronts shown in figure 1d–e strongly suggest the existence of first order phase transitions between different protein configurations. These transitions are intrinsically physical but can be located thanks to the Pareto formalism. Other

authors have studied the tradeoffs related to information spread in complex networks [29]. Different network topologies minimize/maximize the efficiency of routing or enhance/hinder the diffusion of information. Phase transitions are also evident in this example (see figure 3 in [29]). We can consider the entropy associated to the information routed through the network. That entropy can eventually be linked to energy through the Landauer principle [63] so that these transitions might have clear physical interpretations.

A review of MOO literature from the proposed perspective seems necessary now, but each individual case should be studied carefully. Very recent contributions are exploring biology from an MOO perspective, making it a very attractive territory where to apply our insights. But this field can also prove challenging. Following [27] and [32], several tasks (P_1, \dots, P_K) can contribute to the fitness of a species through $F = F(P_1, \dots, P_K)$. Improvements in any P_k might raise the overall fitness justifying an MOO study. But the consequences of the MOO-SOO combination have not been explored. Our framework relies on the integration of the targets that in the case of thermodynamics and other problems happens through a linear combination (as in equation 3). The scenario suggested in [27, 32] becomes interesting because the MOO-SOO collapse imposed by $F = F(P_1, \dots, P_K)$ is not necessarily linear. In our framework SOO optima are always mutually non-dominating so that SOO and MOO problems can be simultaneously solved. This might not be the case for non-linear fitness functions, opening interesting possibilities associated to biological fitness. Further research should address these and other pending issues.

Acknowledgments

We thank the members of the CSL for useful discussions. This work was supported by grants from the Fundación Botín, the European Research Council (ERC Advanced Grant) and by the Santa Fe Institute.

Appendix A: A discussion of thermodynamics as an MOO problem

We have shown how the solutions to an MOO-SOO problem based on a physical system correspond precisely to the canonical ensembles of that system in thermodynamic equilibrium. A crucial step is proving that the microcanonical ensemble reconstructs the Pareto front of the relevant MOO. We devote some space here to better clarify this point.

The reconstruction of the Pareto front through microcanonical ensembles derives from the second law of thermodynamics. Microcanonical ensembles are those that maximize the entropy for a fixed value of internal energy (figure 7a). Each microcanonical ensemble is mapped into the $U - S$ plane through equations 5. All these en-

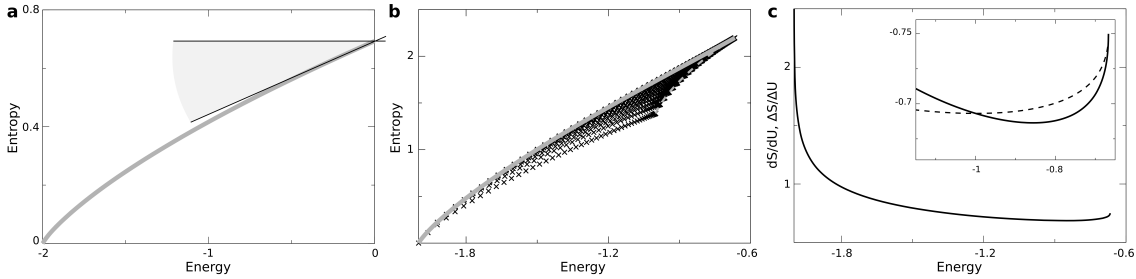


FIG. 6: **Pareto fronts for the Ising and Potts models.** **a** The front of the mean-field Ising model (thick gray line) is convex but ends abruptly revealing a range $\beta \in (0, 1/Jz]$ (gray fan) for which SOOs arrive to the most entropic solution always. **b** A sample of arbitrary distributions $P = \{p_1, p_2, p_3\}$ (black crosses) for the $q = 3$ Potts model is dominated by its Pareto front whose top-right part is concave. This indicates a first order phase transition. **c** That cavity becomes noticeable when analyzing the slope of the front, which is not monotonously decreasing.

sembles together trace a curve that must be a function $S = \bar{S}(U)$. Otherwise, for a value of U two or more values of S would be assigned, and only one of them could be maximum. The lower values would not correspond to any microcanonical ensemble, accordingly.

Consider the situation in which $S = \bar{S}(U)$ increases monotonically. Then a greater internal energy is always associated to a greater entropy, which intuitively makes sense. This bijectivity guarantees that $S = \bar{S}(U)$ matches the corresponding Pareto front. For each $U_j > U_i$ necessarily $\bar{S}(U_j) > \bar{S}(U_i)$, thus in this curve there are not any two $U_i < U_j$ such that $\bar{S}(U_i) > \bar{S}(U_j)$, which would imply $U_i \prec U_j$. Furthermore, any ensemble mapped into a point (U_i, S_i) outside this curve is necessarily dominated by some microcanonical ensemble mapped into $(U_i, \bar{S}(U_i))$ since by definition microcanonical ensembles are such that $\bar{S}(U_i) > S_i$ for that given value U_i . Summing up: i) points along the curve $S = \bar{S}(U)$ are mutually non-dominated and ii) for any physically plausible point (U, S) outside this curve there is at least one point that belongs to the curve and dominates (U, S) . This is the definition of the Pareto front indeed. Once microcanonical ensembles reconstruct the front of the proposed MOO, the collapse into SOOs and phase transitions due to the shape of the front follow naturally because the free energy is minimized in thermodynamic equilibrium.

Some mathematical idealizations of physical systems admit non-monotonically increasing entropies. These often lead to exotic parameterizations such as negative temperatures. Furthermore they do not affect the current theory as we will show now. Consider figures 7b and c regardless of the physical reality of such descriptions. The equilibrium thermodynamics of such hypothetical systems are still well represented by the convex hull of the Pareto front, hence our theoretical framework remains true. Given the definition of dominance, we note that the Pareto front of the relevant MOO problem is still fully reconstructed by the curve $S = \bar{S}(U)$ (thick stretches in figures 7b-c). Non-increasing stretches of $S = \bar{S}(U)$ lay inside a cavity (figure 7b) or after the

global maximum of the function (figure 7c). If they are inside a cavity, such situations never show up in thermodynamic equilibrium, whose canonical ensembles are strictly mapped into the convex hull of the front. These points are bypassed by a first order phase transitions. In the other situation, the slope of the Pareto front at the global maximum (whose limit from below is perfectly reconstructed by the microcanonical ensemble) is necessarily 0, meaning that such situation is only reached at $\beta \rightarrow 0 \Rightarrow T \rightarrow +\infty$. Reaching solutions beyond the global maximum implies considering $\beta = 1/T < 0$, which is not realistic. Thus non monotonously increasing functions $S = \bar{S}(U)$ do not affect the general framework because they are situations that we are not concerned with in thermodynamic equilibrium. For MOO-SOO systems others than thermodynamics we do not rely on microcanonical ensembles, but on the Pareto front straightforward, in which non-dominated regions (including curves that would break the monotonic trend of the front) never show up.

Our work follows closely some ideas from Gibbs [60–62] that did not become so mainstream in the study of statistical mechanics. Gibbs’s *graphic method* relied on the existence of a surface upon which all possible states of a thermodynamic species in equilibrium dwell. This surface is defined by the Gibbs potential $G(p, T) = U + pV - TS$, which plays the role of equation 3 both in thermodynamics and in our theoretical framework. We identify the target functions U , S , and V and the control parameters T and p . The tangent plane at a given point of the surface is defined by a normal vector whose components are precisely related to the pressure and temperature of that equilibrium state [62].

It was argued that an MOO approach might be adequate when the different targets cannot be compared (e.g. if they have different units). In thermodynamics, the control parameters T and p transform different potentials into the same units. At fixed temperature entropy is heat and at fixed pressure volume is work – hence a low entropy and an unoccupied volume are available

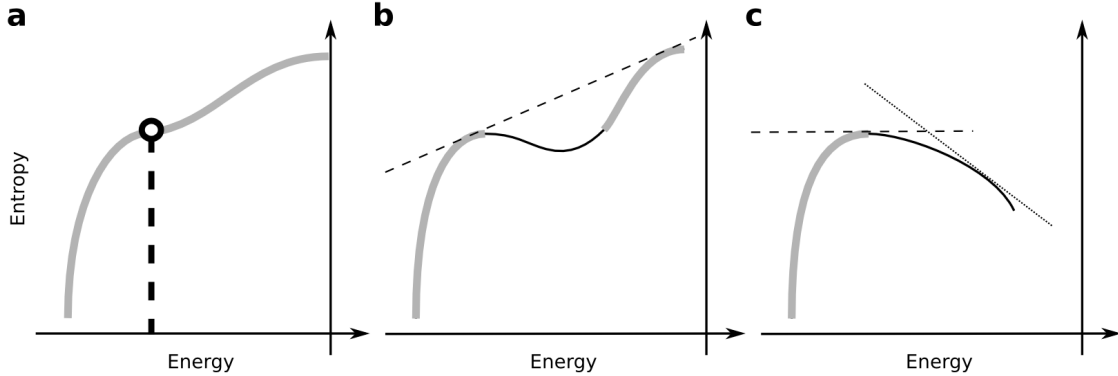


FIG. 7: Laws of thermodynamics and the Pareto front. **a** According to the second law of thermodynamics, at constant internal energy (vertical dashed line) the microcanonical ensemble is the one that maximizes the entropy (and is hence mapped into the open circle in this example). Implementing this maximization for varying energy yields a function on the $U - S$ space that for thermodynamic systems is usually monotonously increasing with U – more energetic systems usually have more entropy. This guarantees that any two points on this curve are mutually non-dominated. There cannot be any point above this curve, thus the obtained curve must be exactly the Pareto front of the corresponding MOO problem. **b** This curve would not match the front only if the microcanonical entropy were not monotonously increasing with U . This is an odd situation in thermodynamics. These non-increasing stretches would necessarily lay inside a cavity (solid black curve) and would never show up in thermodynamic equilibrium. **c** Such situation can also happen beyond the global maximum of the entropy, which is only reached for $T = 0$ (dashed line). Points of the microcanonical entropy beyond this maximum would require $\partial S / \partial U = 1/T < 0$ (i.e. negative temperatures, dotted line). In both **b** and **c** the entropy of microcanonical ensembles still contains the whole Pareto front and, of course, its convex hull.

free energy. All free energy must be utilized to reach the thermodynamic equilibrium [62] so that $G(p, T)$ is minimized and only the convex hull of the Gibbs surface shows up. When changing T or p quasistatically, concavities are bypassed revealing first order phase transitions. Sharp edges are consistently related to second order phase transitions again.

This ingenious picture received renewed attention recently [65, 66] and is connected to the concept of ensemble inequivalence [68]. The Gibbs surface is fabricated thanks to the microcanonical ensemble and it can be convex or concave, while a thermodynamic canonical ensemble can only be convex (note that we use a different convention for concavity/convexity). Whenever G becomes concave both ensembles must diverge geometrically in the $U - V - S$ space. This makes the canonical ensemble non-analytic at the inequivalence points which is reflected as a first order phase transition in the corresponding physical system.

Appendix B: Solving the Ising and Potts models from an MOO perspective

As noted in the main text, the Ising and the Potts models and more general versions of them have been solved using the concept of ensemble inequivalence [69, 70], which is comprehensively explained by the Pareto optimality approach introduced here. We illustrate thermodynamic phase transitions with the Pareto front through these models because of their historical importance and

because they allow a complete analytical treatment. The details of the calculations follow.

d. The mean-field Ising model – a second order phase transition We use a standard mean-field Hamiltonian for the Ising model $H_j = -\frac{J}{2} \sum_{\langle j,k \rangle} s_j s_k$ with J the coupling constant and the sum running over z neighboring spins. We parameterize the system with the probability p that we find the mean-field spin in the *up* state. It becomes easy to write down the entropy and the internal energy of the system in terms of p :

$$\begin{aligned} S &= -p \log(p) - (1-p) \log(1-p), \\ U &= -\frac{Jz}{2} (2p-1)^2. \end{aligned} \quad (B1)$$

Solving this last expression for p , we can also write the entropy as a function of the internal energy alone:

$$\begin{aligned} \bar{S}(U) &= -\frac{1}{2} \{1 + f(U)\} \log \left(\frac{1 + f(U)}{1 - f(U)} \right) \\ &\quad - \log \left(\frac{1 - f(U)}{2} \right), \end{aligned} \quad (B2)$$

with:

$$f(U) \equiv +\sqrt{\frac{-2U}{Jz}}. \quad (B3)$$

Equation B2 (represented in figure 6a) gives us S as a function of U ($S = \bar{S}(U)$) for all possible states that the model can be found into, disregard of whether or not these states correspond to thermodynamic equilibrium

situations or to microcanonical ensembles. Because for this model equation B2 is a function, for each U $\bar{S}(U)$ is also maximal – i.e. every state of the system corresponds to a microcanonical ensemble itself. This is luckily valid for this one model, but not necessarily true in a general case.

This curve also constitutes the Pareto front of the corresponding MOO problem (minimizing U and maximizing S from equations 5), as is expected given the correspondence between the microcanonical ensembles and Pareto optimal solutions. Let us analyze the Pareto optimality of equation B2. First we note that $\bar{S}(U)$ is only real and well defined for $U \in [-Jz/2, 0]$, the range of available energies for the model. In this range:

$$\frac{d\bar{S}}{dU} = -\frac{1}{2}f'(U)\log\left(\frac{1+f(U)}{1-f(U)}\right) > 0, \quad (\text{B4})$$

thus $\bar{S}(U)$ is monotonously increasing, which guarantees that its points in the $U - S$ plane do not dominate each other regarding energy minimization and entropy maximization. Because this curve comprises everything that is possible in the system under research and because its constituting points are mutually non-dominated, it must be the Pareto front itself.

Besides, $\frac{d\bar{S}}{dU}$ is positive and monotonously decreasing for $U \in (-Jz/2, 0)$; thus there are not concavities in the Pareto front: we rule out first order phase transitions. We can also rule out second order phase transitions in the interior of $U \in (-Jz/2, 0)$ because the derivative is well defined everywhere. Second order phase transitions are thus restricted to $U = -Jz/2$ or $U = 0$. We inspect $\frac{d\bar{S}}{dU}$ as U tends to these points. After some algebra we arrive to:

$$\lim_{U \rightarrow 0^-} \frac{d\bar{S}}{dU} = \frac{1}{Jz}. \quad (\text{B5})$$

and:

$$\lim_{U \rightarrow (-Jz/2)^+} \frac{d\bar{S}}{dU} = +\infty. \quad (\text{B6})$$

As we saw in the results section, for the SOO posed at temperature $T = 1/\beta$ we typically reach points of the Pareto front where their tangent matches the slope of the corresponding $\tau_\beta(F) = \{(U, S) | S = \beta U - \beta F\}$. The derivative $\frac{d\bar{S}}{dU}$ as we approach $U = -Jz/2$ is infinite, meaning that we will reach this end of the Pareto front only at $\beta \rightarrow \infty$ (zero temperature). There is not any remarkable behavior here. At the other end of the Pareto front the derivative is not 0, but a finite positive number. This means that already for $\beta = \frac{1}{Jz}$ the free energy optimum – i.e. the SOO solution – is located at the upper right end of the front which corresponds to the state with more entropy and energy. If we further decrease β we will not be reaching any novel solutions: the SOO optima remain the most entropic state of the system. Going back to the well behaved range of β , as we increase it

above $\frac{1}{Jz}$ the SOO solutions begin to roll over the Pareto front continuously. The transition between a persistent solution for $\beta \in (0, 1/Jz]$ and a varying solution in the regime $\beta \in (1/Jz, +\infty)$ implies a discontinuity in the derivative of any order parameter. This is analogous to the cases illustrated in figure 3 of the main text, and is associated to second order phase transitions as the one that we know that the mean-field Ising model undergoes at precisely $\beta = \beta^c \equiv \frac{1}{Jz}$.

e. *The mean-field Potts model – a first order phase transition.* We repeat the same operations with the Bragg-Williams approximation to the Potts model. This has been solved somewhere else [71] using other methods. This choice of implementing the mean-field presents first order phase transitions for any $q \geq 3$, where q is the number of available states for each spin. For a discussion of the Braggs-Williams against other mean-field approaches to the Potts model see [72].

Following [71], we write down the entropy and energy of the system:

$$\begin{aligned} S &= -\sum_{j=1}^q p_j \log(p_j), \\ U &= -\frac{zJ}{2} \sum_{j=1}^q p_j^2; \end{aligned} \quad (\text{B7})$$

with J and z still the coupling and the number of neighbors. Now U and S are parameterized by the probabilities p_j ($j = 1, \dots, q$) of finding a spin in each of the $q \geq 3$ states. The normalization $\sum_j p_j = 1$ means that there are $q-1$ parameters and we cannot write $S = \bar{S}(U)$ as before unless we make some assumption. Let us prefer one arbitrary state (say $j = 1$) over the others. Let us call p to the probability of finding a spin in that preferred state, and let us further assume that any other state is equally likely $p_{j'} = (1-p)/(q-1)$, now with $j' = 2, \dots, q$. This is analytically justified in the literature [71] and later by our arguments about Pareto dominance. We note that, unlike for the Ising model, states compatible with the premises of the system will not usually be constrained to a curve because we have too many degrees of freedom. In figure 6b (main text) we represent a sample of valid points for $q = 3$: all of them can happen in theory (they are mathematically valid descriptions of the system). A few of them Pareto dominate some others thus not all of these configurations will be reached in thermodynamic equilibrium.

Thanks to the previous symmetry breaking to favor one state over the others we can write down the following curve:

$$\begin{aligned} \bar{S}(U) &= -\frac{1+f_q(U)}{q} \log\left(\frac{(q-1)(1+f_q(U))}{q-1-f_q(U)}\right) \\ &\quad -\log\left(\frac{q-1-f_q(U)}{q(q-1)}\right). \end{aligned} \quad (\text{B8})$$

This is the counterpart of equation B2 only now:

$$f_q(U) \equiv \sqrt{(1-q) \left[1 + \frac{2qU}{zJ} \right]}. \quad (\text{B9})$$

Equation B8 is represented in figure 6b of the main text for $q = 3$. We can appreciate that it is monotonously growing as a function of U : its points are mutually non-dominated and constitute the Pareto front. The fact that there is not any point in the previous sample that Pareto dominates any point in this curve suggests that our symmetry breaking hypothesis (favoring one spin state over the others) is correct. It can be analytically proved, indeed [71]. Although it is visually difficult to appreciate, a concavity exists in the upper right part of the Pareto front. This becomes more obvious when analyzing $\frac{d\bar{S}}{dU}$ (figure 6c of the main text), which is not monotonously decreasing.

Most of the Pareto front is continually visited: as we vary β , the SOO solutions roll over its convex lower-left part. It can be shown once more that the less energetic extreme of the front is reached only for $\beta \rightarrow +\infty$ and $T = 0$, so that there is not any remarkable feature in that temperature range. Once again, it exists a value β^* below which the solution is persistently the most entropic one. At exactly $\beta = \beta^*$ that solution coexists with another one in the convex part of $\bar{S}(U)$.

To locate β^* we plot $\frac{d\bar{S}}{dU}$ and we compare it to the slope $\frac{\Delta S}{\Delta U}$ of the straight line that connects the top-right extreme with other points along the Pareto front (main text, figure 6c, inset). Where both functions intersect we have identified the phases that coexist. The straight line that connects these phases has slope β^* precisely. We collect β^* for the Potts models with different parameter values q in figure 8b. These results match those known from the literature [71].

Because the two coexisting solutions are far away in the Pareto front, at $\beta = \beta^*$ these systems undergo a drastic change – as opposed to the continuous transition from the Ising model. This is similar to the first order phase transition situation illustrated in figure 4 of the main text. This is the kind of phase transition that we know that our model presents.

In figure 8 we represent the Pareto front for many values of q . We observe that solutions for q dominate solutions for any $q' < q$, leading to the interesting (while trivial) observation that an instance with higher q does not spontaneously decay towards one with less available states by setting some $p_{j'} = 0$. This is well known for the Potts model, but such an interesting scenario should not be discarded in general for a different problem, and the Pareto front could provide a formalism to detect such a possibility.

[1] Schuster P, Optimization of multiple criteria. *Complexity* **18**, 5-7 (2012).

[2] Murray CD, The physiological principle of minimum work. I. The vascular system and the cost of blood volume. *Proc. Nat. Acad. Sci.* **12**, 207-213 (1926).

[3] West GB, Brown JH, Enquist BJ, A General Model for the Origin of Allometric Scaling Laws in Biology. *Science* **276** 122-126 (1997).

[4] West GB, Brown JH, Enquist BJ, A general model for the structure and allometry of plant vascular systems. *Nature* **400** 664-667 (1999).

[5] Gafiychuk VV, Lubashevsky IA, On the Principles of the Vascular Network Branching. *J. Theor. Biol.* **212**, 1-9 (2001).

[6] Gastner MT, Newman MEJ, Optimal design of spatial distribution networks. *Phys. Rev. E* **74**, 016117 (2006).

[7] Cuntz H, Borst A, Segev I, Optimization principles of dendritic structure. *Theor. Biol. Med. Model.* **4**, 21 (2007).

[8] Pérez-Escudero A, de Polavieja GG, Optimally wired subnetwork determines neuroanatomy of *Caenorhabditis elegans*. *Proc. Nat. Acad. Sci.* **104**(43), 17180-17185 (2007).

[9] Casvalho R, Buzna L, Bono F, Gutiérrez E, Wolfram J, Arrowsmith D, Robustness of trans-European gas networks. *Phys. Rev. E* **80**, 016106 (2009).

[10] Bassett DS, Greenfield DL, Meyer-Lindenberg A, Weinberger DR, Moore SW, Bullmore ET, Efficient Physical Embedding of Topologically Complex Information Processing Networks in Brains and Computer Circuits. *PLoS Comput. Biol.* **6**(4), e1000748 (2010).

[11] Hasenstaub A, Otte S, Callaway E, Sejnowski TJ, Metabolic cost as a unifying principle governing neuronal biophysics. *Proc. Nat. Acad. Sci.* **107**(27), 12329-12334 (2010).

[12] Cuntz H, Forstner F, Borst A, Häusser M, One Rule to Grow Them All: A General Theory of Neuronal Branching and Its Practical Application. *PLoS Comput. Biol.* **6**(8), e1000877 (2010).

[13] Barthélémy M, Spatial networks. *Phys. Rep.* **499**(1), 1-101 (2011).

[14] Dennett DC, *Darwin's dangerous idea*. Touchstone, New York (1995).

[15] Coello CA, Evolutionary Multi-Objective Optimization: A Historical View of the Field. *IEEE Comput. Intell. M.* **1**(1), 28-36 (2006).

[16] Fonseca CM, Fleming PJ, An Overview of Evolutionary Algorithms in Multiobjective Optimization. *Evol. Comput.* **3**, 1-16 (1995).

[17] Dittes FM, Optimization on Rugged Landscapes: A New General Purpose Monte Carlo Approach. *Phys. Rev. Lett.* **76**(25), 4651-4655 (1996).

[18] Zitzler E, *Evolutionary Algorithms for Multiobjective Optimization: Methods and Applications*, A dissertation submitted to the Swiss Federal Institute of Technology. PhD Thesis, Eidgenössische Technische Hochschule Zürich (1999).

[19] Konak A, Coit DW, Smith AE, Multi-objective optimization

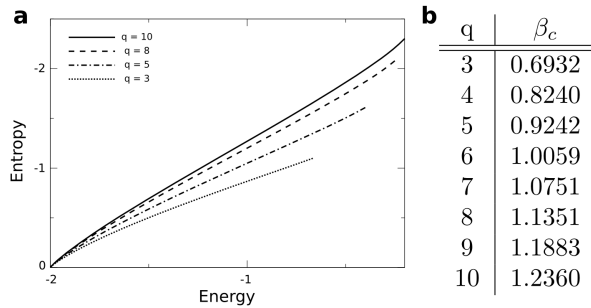


FIG. 8: **Pareto front for the mean-field Potts model with different q .** **a** Pareto fronts of the Potts model for $q = 3, 5, 8, 10$. Although hardly noticeable, all these fronts have got concave stretches towards their upper-right ends. This indicates that all of them undergo first order phase transitions from the most disordered state to a more ordered phase where symmetry has been broken to favor just one of the states. A Pareto front for q dominates the Pareto front for every $q' < q$ indicating that this system will never leave empty one of its available states spontaneously, except in the most ordered state in which all spins are aligned. **b** Inverse temperature at which the mean-field Potts model presents its first order phase transition for $q = 3, \dots, 10$. The results match perfectly those from the literature [71].

tion using genetic algorithms: A tutorial. *Reliab. Eng. Syst. Safe.* **91**(9), 992-1007 (2006).

[20] Arrow KJ, Uncertainty and the welfare economics of medical care. *Am. Econ. Rev.* **53**(5), 941-973 (1963).

[21] Steuer RE, Na P, Multiple Criteria Decision Making Combined with Finance: A Categorized Bibliographic Study. *Eur. J. Oper. Res.* **150**(3), 496-515 (2003).

[22] Cutello V, Narzisi G, Nicosia G, A multi-objective evolutionary approach to the protein structure prediction problem. *J. R. Soc. Interface* **3**(6), 139-151 (2006).

[23] Druckmann S, Banitt Y, Gidon A, Schüermann F, Markram H, Segev I, A novel multiple objective optimization framework for constraining conductance-based neuron models by experimental data. *Front. Neurosci.* **1**(1), 7-18 (2007).

[24] Kennedy MC, Functional-structural models optimize the placement of foliage units for multiple whole-canopy functions. *Ecol. Res.* **25**, 723-732 (2010).

[25] Grimme C, Lepping J, Papaspyrou A, Parallel predator-prey interaction for evolutionary multi-objective optimization. *Nat. Comput.* **11**, 519-533 (2012).

[26] Noor E, Milo R, Efficiency in Evolutionary tradeoffs. *Science* **336**, 1114 (2012).

[27] Shoval O, Sheftel H, Shinar G, Hart Y, Ramote O, Mayo A, Dekel E, Kavanagh K, Alon U, Evolutionary tradeoffs, Pareto Optimality, and the Geometry of Phenotype Space. *Science* **336** 1157-1160 (2012).

[28] Schuetz R, Zamboni N, Zampieri M, Heinemann M, Sauer U, Multidimensional Optimality of Microbial Metabolism. *Science* **36**, 601-604 (2012).

[29] Goñi J, Avena-Koenigsberger A, de Menizabal NV, van den Heuvel M, Betzel R, Sporns O, Exploring the morphospace of communication efficiency in complex networks. *PLoS ONE* **8**, e58070 (2013).

[30] Priester C, Schmitt S, Peixoto TP, Limits and trade-offs of Topological Network Robustness. *PLoS ONE* **9**(9), e108215 (2014).

[31] Higuera C, Villaverde AF, Banga JR, Ross J, Mora F, Multi-Criteria Optimization of Regulation in Metabolic Networks. *PLoS ONE* **7**(7), e41122 (2012).

[32] Szekely P, Sheftel H, Mayo A, Alon U, Evolutionary Tradeoffs between Economy and Effectiveness in Biological Homeostasis Systems. *PLoS Comput. Biol.* **9**(8), e1003163 (2013).

[33] Otero-Muras I, Banga JR, Multicriteria global optimization for biocircuit design. *BMC Syst. Biol.* **8**, 113 (2014).

[34] Wilson LA, Moore MD, Picarazzi JP, Miquel SDS, Parallel genetic algorithm for search and constrained multi-objective optimization. Parallel and Distributed Processing Symposium, Proceedings. 2004.

[35] Denysiuk R, Silva CJ, Torres DFM, Multiobjective approach to optimal control for tuberculosis model. *Optim. Method. Soft.* doi: 10.1080/10556788.2014.994704 (2014).

[36] Jaynes ET, Information theory and statistical mechanics. *Phys. Rev.* **4**, 620-630 (1957).

[37] Harte J, *Maximum entropy and ecology: a theory of abundance, distribution, and energetics*. Oxford University Press (2011).

[38] Mora T, Bialek W, Are biological systems poised at criticality? *J. Stat. Phys.* **144**(2), 268-302 (2011).

[39] Ball P, *Critical mass: How one thing leads to another*. Macmillan (2004).

[40] Castellano C, Fortunato S, Loreto V, Statistical physics of social dynamics. *Rev. Mod. Phys.* **81**(2), 591 (2009).

[41] Fontana W, Schnabl W, Schuster P, Physical aspects of evolutionary optimization and adaptation. *Phys. Rev. E* **40**, 3301-3321 (1989).

[42] Prügel-Bennett A, Shapiro JL, Analysis of Genetic Algorithms Using Statistical Mechanics. *Phys. Rev. Lett.* **72**(9), 1305-1309 (1994).

[43] Asselmeyer T, Ebeling W, Rosé H, Evolutionary strategies of optimization. *Phys. Rev. E.* **56**(1), 1171-1180 (1997).

[44] Bornholdt S, Genetic algorithm dynamics on a rugged landscape. *Phys. Rev. E* **57**(4), 3853-3860 (1998).

[45] Martin OC, Monasson R, Zecchina R, Statistical mechanics methods and phase transitions in optimization problems. *Theor. Comp. Sci.* **265**, 3-67 (2001).

[46] Bialek W, *Biophysics: searching for principles*. Princeton University Press (2013).

[47] Hogg T, Huberman BA, Williams CI, Phase transitions and the search problem. *Artif. Intell.* **81**, 1-15 (1996).

[48] Gent IP, Walsh T, The TSP phase transition, *Artif. Intell.* **88**, 349-358 (1996).

[49] Reimann A, Ebeling W, Ensemble-based control of evolutionary optimization algorithms. *Phys. Rev. E.* **65**, 046106 (2002).

[50] Banga JR, Optimization in computational systems biology. *BMC Syst. Biol.* **2**, 47 (2008).

[51] Nehert RA, Shraiman BI, Statistical Genetics and Evolution of Quantitative Traits. *Rev. Mod. Phys.* **83**(4), 1283-1300 (2011).

[52] Mathias N, Gopal V, Small Worlds: how and why. *Phys. Rev. E* **63**(2), 021117 (2001).

[53] Ferrer i Cancho R, Solé RV, Optimization in complex networks. *Lect. Notes Phys.* **625**, 114-125 (2003).

[54] Colizza V, Banavar JR, Maritan A, Rinaldo A, Network Structures from Selection Principles. *Phys. Rev. Lett.*

92(19), 198701-1 (2004).

[55] Newman MEJ. *Networks*. Oxford University Press (2010).

[56] Ferrer i Cancho R, Solé RV, Least effort and the origins of scaling in human language. *Proc. Natl. Acad. Sci.* **100**(3), 788-791 (2003).

[57] Prokopenko M, Ay N, Obst O, Polani D, Phase transitions in least-effort communications. *J. Stat. Mech.* **11**, P11025 (2010).

[58] Dickman R, Moloney NR, Altmann EG, Analysis of an information-theoretic model for communication. *J. Stat. Mech.* **2012**(12), P12022 (2012).

[59] Solé RV, Seoane LF, Ambiguity in Language Networks. *Linguist. Rev.* **32**(1), 5-35 (2014).

[60] Gibbs JW, Graphical Methods in the Thermodynamics of Fluids. *Trans. Conn. Acad.* **2**, 309-342 (1873).

[61] Gibbs JW, A Method of Geometrical Representation of the Thermodynamic Properties of Substances by Means of Surfaces. *Trans. Conn. Acad.* **2**, 382-404 (1873).

[62] Maxwell JC, *Theory of Heat*. Longmans, Green, and Co. (1904).

[63] Landauer R, Irreversibility and heat generation in the computing process. *IBM J. Res. Dev.* **5**(3), 183-191 (1961).

[64] Seoane LF, Solé R, Phase transitions in Pareto optimal complex networks. In print *Phys. Rev. E*, 10.1103/Phys-RevE.00.002800, <http://arxiv.org/abs/1505.06937> (2015).

[65] Varchenko AN, Evolutions of convex hulls and phase transitions in thermodynamics. *J. Sov. Math.* **52**(4), 3305-3325 (1990).

[66] Aicardi F, On the classification of singularities in thermodynamics. *Phys. D* **158**, 175-196 (2001).

[67] Bouchet F, Barr J, Classification of phase transitions and ensemble inequivalence, in systems with long range interactions. *J. Stat. Phys.* **118**(5-6), 1073-1105 (2008).

[68] Touchette H, Ellis RS, Turkington B, An introduction to the thermodynamic and macrostate levels of nonequivalent ensembles. *Phys. A* **340**, 138-146 (2004).

[69] Bertalan Z, Kuma T, Matsuda Y, Nishimori H, Ensemble Inequivalence in the Ferromagnetic p -spin Model in Random Fields. *J. Stat. Mech.* **1**, P01016 (2011).

[70] Costeniuc M, Ellis RS, Touchette H, Complete Analysis of Phase Transitions and Ensemble Equivalence for the Curie-Weiss-Potts Model. *J. Math. Phys.* **46**, 063301 (2005).

[71] Kihara T, Midzuno Y, Shizume T, Statistics of Two-Dimensional Lattices with Many Components. *J. Phys. Soc. Jpn.* **9**(5), 681-687 (1954).

[72] Wu FY, The Potts model. *Rev. Mod. Phys.* **51**(1), 235-267 (1982).